Mechanism of nonrandom pattern formation of polar-conjugated molecules in a partial wetting regime

Martin Brinkmann,[1,2] Sabine Graff,[1] and Fabio Biscarini[2,*]
[1]*Institut Charles Sadron, CNRS, 6 rue Boussingault, 67083 Strasbourg, France*
[2]*Consiglio Nazionale delle Ricerche-ISMN, Sezione di Bologna, Via P. Gobetti 101, I-40129 Bologna, Italy*
(Received 28 June 2001; revised manuscript received 8 July 2002; published 30 October 2002)

An original nucleation and growth process has been investigated for vacuum-deposited films of a polar-conjugated molecule, tris-(8-hydroxyquinoline) aluminum (III) (Alq_3), onto the apolar H-terminated Si(100). Homogeneous nucleation of amorphous Alq_3 clusters is restricted to the early stage of deposition and is characterized by a large critical nucleus size $i=5$, as determined from the dependence of the density of stable nuclei N on deposition rate κ. Alq_3 clusters grow in a partial wetting regime to form correlated droplet patterns. For moderate deposition rates around 1 nm/min, patterns exhibit both (i) a typical scale invariance of the droplet size distribution with coverage and substrate temperature and (ii) strong correlations between the size and position of the droplets. Both these characteristics result from the absence of coarsening—e.g., Ostwald ripening, secondary nucleation, and coalescence during growth. Spatial correlations are analyzed by using Voronoi tesselation, which demonstrates the validity of a phenomenological capture zone model for correlated growth. Correlations emerge in the early stage of growth via direct ripening and further develop during growth by diffusive interactions between domains. Direct ripening manifests itself by the introduction of a minimum cutoff distance between droplets, which causes a significant narrowing of the droplet size distribution. During growth, diffusive interactions between droplets cause their centers of mass to move towards empty depleated areas, which results in enhanced spatial correlations. This peculiar nucleation and growth mechanism allows one to obtain droplet patterns where the interdroplet distance and droplet size can be tuned independently via deposition temperature and time.

DOI: 10.1103/PhysRevB.66.165430 PACS number(s): 61.43.Hv, 68.37.Ef, 81.15.Ef, 78.66.Qn

I. INTRODUCTION

Thin films made of electroactive molecules, such as π-conjugated molecules and coordination compounds, play a major role in material science nowadays. Mastering the morphology and structure of molecular thin films in devices such as organic light emitting diodes (OLEDs)[1] and organic field effect transistors (OFETs)[2] has progressively emerged as a crucial issue since relevant transport and optical properties are strongly dependent on the degree of order achieved at multiple length scales, ranging from nanometers to micrometers.[3] In epitaxial growth,[4–8] molecular order results from the interplay between the molecule-substrate and intermolecular interactions.[5] However, neither the size of domains nor the spatial arrangement of the domains can be easily controlled, mainly because growth occurs in nonequilibrium conditions.[9,10] In addition, coarsening phenomena during growth (static coalescence, Ostwald ripening, and nucleation during growth) prevent the formation of ordered patterns.[11] There are systems, albeit not made of conjugated molecules, where either coarsening is suppressed or contributes to the emergence of spatial correlations among the domains. Such spatial correlations are due to competing interactions; examples are magnetic bubbles, Langmuir-Blodgett binary mixtures, block copolymers, polymer blends, and quantum dots.[12]

In our earlier work,[13] we showed that spatial correlations can be achieved also in thin films made of a polar-conjugated molecule, viz., tris-(8-hydroxyquinoline) aluminum (III) (Alq_3),[1,14,15] sublimed onto an apolar surface, viz., H-passivated Si(100). Thin films consist of spherical-cap-shaped droplets growing in a partial wetting regime. A typical example is shown in Fig. 1. Alq_3 droplet patterns remind of breath figures (formed when a vapor condenses on a cold surface in a nonwetting or partial-wetting regime[16–20]), but some of their features make the system Alq_3/H-terminated Si(100) peculiar and interesting. The most interesting characteristic of this system is the absence of coarsening phenomena during growth. As a result, Alq_3 patterns are stabilized in a nearly hexagonal packing of domains at full coverage.[13] Another interesting feature is the emergence of a narrow distribution of domain size, which can be rescaled by its mean value onto a universal curve (self-similarity). It is important to remark that the characteristic length scale of the spatial correlations (which represents the interdroplet distance) is not the result of either rupture or spinodal dewetting of a homogeneous film, but it appears in the early stage of growth.

The fundamental question we address in this paper is the origin of the spatial correlations. In addition, we extend our previous study with the investigation of the nucleation process and how it affects droplet growth. We determine the critical nucleus size of amorphous Alq_3 clusters. The spatial correlations, which are analyzed using Voronoi tesselation, are shown to emerge in the nucleation stage and to evolve during subsequent growth of the droplets because of diffusive interactions between growing droplets. Our results conciliate the phenomenological capture zone (CZ) model developed by Mulheran and Blackman[21,22] with earlier models by Venables and Ball,[23] and support a scenario where homoge-

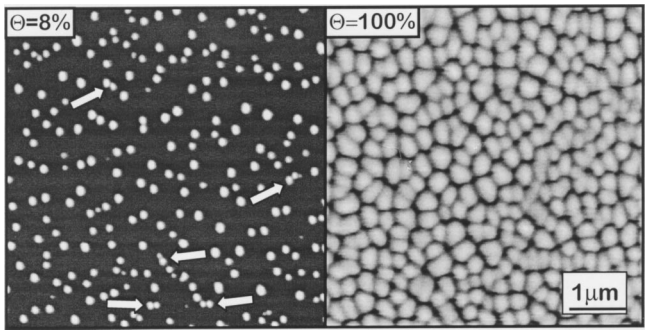

FIG. 1. Effect of coverage on the morphology of Alq_3 thin films grown onto H-passivated Si(100) substrate at $T_s = 100\,°C$. The deposition rate was kept at a value of approximately 1.0 nm/min. The scanned area corresponds to $6.4 \times 6.4\ \mu m^2$. Arrows point at close-lying pairs of Alq_3 droplets.

neous nucleation[24] is followed by direct ripening to yield a nonrandom pattern of stable nuclei with a characteristic distance and a narrow-size distribution. In this framework, we explain both the spatial correlations existing between neighboring domains and the scale invariance in time of the domain size distribution.

Our paper is organized as follows: In Sec. II we describe the thin-film growth conditions, as well as the data acquisition using scanning force microscopy (SFM) and scanning electron microscopy (SEM) and image analysis. In Sec. III we present the results which are discussed in Sec. IV. In Sec. V we summarize the main conclusions.

II. EXPERIMENT

Alq_3 thin films have been grown by high-vacuum sublimation (base pressure 10^{-7} mbar) at a constant rate of 1.2 ± 0.1 nm/min onto passivated Si(100) surfaces. The starting material was purchased from Aldrich (98%) and was purified by entrainer sublimation. Clean Si(100) substrates (Wacker Chemitronics, Germany) were passivated by dipping in 10% HF solution for 1 min and subsequently rinsed with deionized water for 2 min prior to vacuum conditioning (few minutes). As demonstrated in previous studies, such passivated surfaces recover the native oxide layer in the time scale of tens of hours.[25] We therefore exclude any significant reoxidation of the passivated surface during film deposition under high vacuum which is completed within a couple of hours. Deposition rate and nominal film thickness h were calibrated on a quartz microbalance placed near the sample by measuring the effective thickness with SFM on micropatterned thin films. Substrate temperatures above 150 °C could not be used since desorption of Alq_3 becomes dominant.

We observed that maintaining the films under high vacuum ($1-4\times10^{-7}$ mbar) for several hours after deposition results in a significant crystallization of the amorphous films. A texture with needles lying in the plane of the substrate, similar to that formed onto ultraoriented poly(tetrafluoroethylene) substrates appears.[26] This crystallization process did not occur when the films were quenched under primary vacuum immediately after deposition. For the study of the rate dependence of the nucleation density N, the substrate temperature was rapidly quenched to room temperature (10 °C/min) by using a nitrogen cooling system in order to avoid coarsening phenomena.

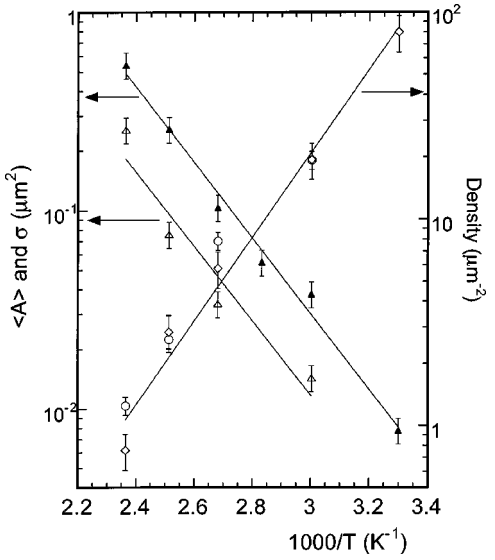

FIG. 2. Arrhenius plot for the mean grain area $\langle A \rangle$ (solid triangles) and statistical variance σ (open triangles) at full coverage ($\Theta \approx 100\%$) and for the grain density per unit surface, N, for films of thickness 100 nm (open diamonds) and 10 nm (open circles).

The amorphous nature of the films has been confirmed by x-ray diffraction for T_s in the range 30–150 °C. The morphology was investigated by contact-mode SFM using soft Si_3N_4 cantilevers (spring constant 0.03–0.06 N/m) with the smallest load forces. SEM imaging was performed on a Hitachi 2300s. Samples for SEM analysis were coated with a thin gold film using a Balzers SCD040.

Image analysis was carried out with SXM-IMAGE (National Institute of Health, Bethesda, MD) and SPIP96 (Danish Institute of Fundamental Metrology, Lingby, Denmark) softwares. Statistics of droplet size were achieved on samples of ca. 400–500 droplets, and convergence of the distribution was checked during counting procedure. Voronoi tesselation was performed by using VOROGLIDE software[27] on SPM topographic images of size 512×512 pixels. The samples used for tesselation contained 250–300 domains, and the convergence of the statistic was followed during the counting procedure. The simulations of random froths were performed by using DIRICHLE software.[28]

III. RESULTS

A. Activation energy and coverage dependence

From the analysis of AFM images, as in Fig. 1, it emerges that the droplet density N (in terms of the number of droplets per unit area) versus inverse T_s decreases exponentially with an activation energy $E_N = 0.39 \pm 0.04$ eV (Fig. 2). The mean projected area of the droplets, $\langle A \rangle$, also follows an Arrhenius law, with activation energy $E_A = 0.36 \pm 0.04$ eV. Within the experimental errors, $E_N = E_A$, in agreement with the fact that $\langle A \rangle \propto 1/N$ at complete coverage $\Theta = 100\%$.

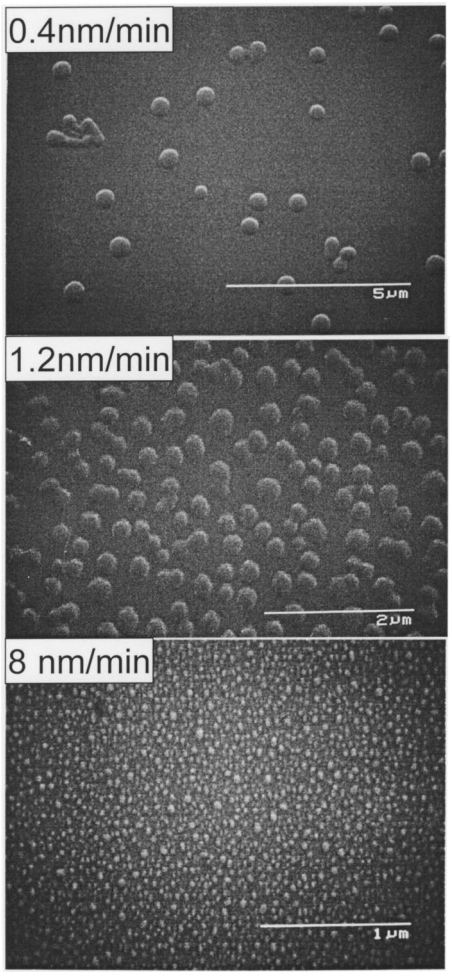

FIG. 3. SEM micrographs of Alq_3/Si(100) thin films grown at $T_s = 125\,^{\circ}C$ for various deposition rates in the range 0.1–8 nm/min. The film thickness is in the range 10–15 nm, which corresponds in all cases to a coverage Θ below 50%.

At fixed T_s, a logarithmic variation of N with coverage is observed. For instance at $T_s = 100\,^{\circ}C$, N increases from 4.8 to 7.8 droplets/μm^2 in the coverage range from 8% to 100% (this range corresponds to a nominal film thickness h between 2 and 100 nm). Given the square dependence of N versus the deposition rate κ (see the following section), the observed variation of N with Θ is ascribed to the variation of deposition rate κ from sample to sample (κ varied between 0.8 and 1.3 nm/min). Accordingly, nucleation is primarily restricted to the early stage of deposition ($\Theta < 8\%$), underlining the absence of significant coarsening phenomena. In the following, Alq_3 deposition onto H-passivated Si(100) will be described in classical terms of nucleation and growth, the two processes occurring at different time scales. This allows us to identify the activation energy E_N as the activation energy for nucleation of amorphous Alq_3 clusters.

B. Primary nucleation

Not only is the growth of Alq_3 onto Si(100) controlled by the substrate temperature T_s, but also by the rate of deposition κ. The sequence of SEM micrographs in Fig. 3 shows

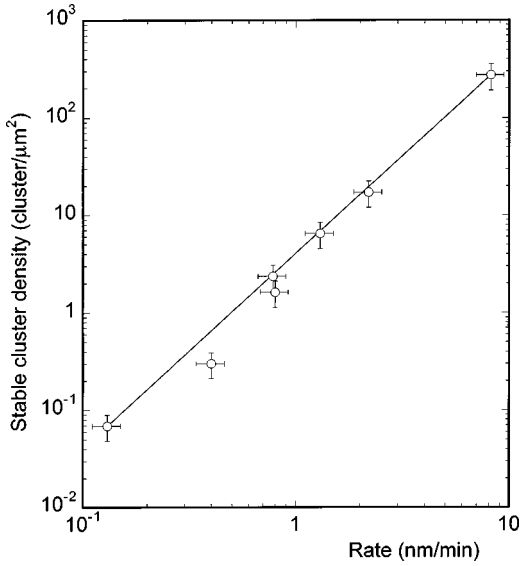

FIG. 4. Rate dependence of the density of Alq_3 droplets per unit surface for thin films grown at $T_s = 125\,^{\circ}C$ onto H-passivated Si(100) substrate. The solid line corresponds to the fit of the experimental data with a power law. Error bars on the deposition rate are estimated from the fluctuations of the deposition rate during sublimation which lie in the range 0.05–0.1 nm/min. Error bars on the density of Alq_3 droplets are estimated from a set of two to three experimental data points obtained at a fixed rate.

the typical evolution of the morphology for Alq_3/Si(100) as a function of increasing deposition rate κ (0.4–8.0 nm/min) at fixed T_s and for low coverage. It is found that N varies between $7 \times 10^{-2}/\mu m^2$ and $2.7 \times 10^2/\mu m^2$ for κ in the range 0.1–8.2 nm/min. The number of nuclei per unit area, N, increases with increasing κ as a power law (Fig. 4), viz., $N \propto \kappa^{\delta}$ with $\delta = 2.00 \pm 0.05$. For comparison, δ exponents reported for nucleation of metal clusters at a surface are typically < 1.[29,30]

The κ dependence of the cluster density allows us to estimate the critical nucleus size i. By definition, clusters with size $j > i$ tend to grow whereas for $j \leq i$ they tend to dissociate.[11] Typically, a small critical nucleus size ($i = 1$ or 2) results in island growth.[11,24] The power-law dependence of N vs κ with an exponent $\delta > 1$ was derived by Venables and co-workers in the frame of the rate-equation formalism[11,30,31] assuming that condensation on the substrate is incomplete. Two regimes of incomplete condensation have been considered for three-dimensional (3D) clusters namely, (i) extreme incomplete condensation which yields $\delta = 2i/3$ and (ii) initially incomplete condensation which gives $\delta = 2i/5$. In the former regime, clusters grow upon direct incorporation of impinging molecules on the cluster surface, whereas in the latter the cluster growth is mainly controlled by diffusion of molecules on the substrate surface. Since the kinetics of droplet growth is successfully modeled by assuming that material is incorporated by both surface diffusion and direct impingement on the droplet surface,[13] we will consider that initially incomplete condensation applies to the case of Alq_3/Si(100), which yields $i = 5$.

The rate-equation formalism also predicts the activated character of N.[30] By combining the results in Figs. 2 and 3, N can be written as[11]

$$N \propto \kappa^{\delta} \exp(\beta E_N), \tag{1}$$

where $E_N = 2[E_5/5 + E_{\mathrm{des}}]$, and E_5 and E_{des} are the binding energy to a cluster of size $i=5$ and the activation energy of desorption, respectively.

In strong contrast to other systems like sexithiophene on mica,[9,10] the present growth mechanism is not controlled by molecular diffusion on the surface. Additional experiments on desorption of Alq_3 via, e.g., thermal desorption spectroscopy are in progress in order to determine the activation energy for desorption of Alq_3 on Si(100).

The large critical nucleus size in the case of Alq_3 with respect to inorganic systems arises because of smaller intermolecular interactions (dipolar and van der Waals) and the weak substrate-overlayer interactions at play. Furthermore, the large value of i found in our case explains the absence of continuous nucleation during growth: the high supersaturation required to nucleate Alq_3 clusters is statistically unlikely to be attained within the depleation zones around the growing clusters, and it is therefore consistent with the logarithmic variation of N vs coverage Θ.

C. Capture zone and Voronoi analysis of the size distribution

In Ref. 13, we evidenced that the distributions of the projected area of the Alq_3 droplets exhibit a self-similar character: at fixed deposition rate $\tau = 1$ nm/min, all the droplet size distributions (DSD's) obtained for different values of Θ and T_s were found to collapse onto a universal curve (see Fig. 4 in Ref. 13). The analysis of moments suggests that the DSD is χ^2 type, and we fit the data to a Γ distribution $G_p(x) = (p^{p-1}/\Gamma_p) x^{p-1} \exp(-px)$. A large value of $p = 10 \pm 2$ was found from the best fit and is presently attributed to the noncoarsening character of growth.[13]

A Γ distribution is also predicted by the recent model of the capture zone developed by Mulheran and Blackman for the analytical form of the DSD.[21,22] The CZ model is based on the assumptions that (i) islands grow at a rate proportional to their CZ area A_{CZ} and (ii) the mosaic of CZ's is time invariant. We used Voronoi tesselation on the experimental data to demonstrate the validity of the CZ model and quantify the nonrandom character of the droplet patterns. Voronoi mosaics on images were taken for various samples grown under different conditions. In Fig. 5, we show the result of Voronoi tessellation performed on a 5-nm thin film grown at $T_s = 100\,^{\circ}\mathrm{C}$ and deposition rate $\kappa = 1.0$ nm/min.

In Fig. 6(a) we have plotted $A^{3/2}$ (proportional to the volume, hence to the mass) as a function of the computed CZ area for a set of 250 droplets. For ease of comparison, both axes were renormalized with respect to the mean values $\langle A^{3/2} \rangle$ and $\langle A_{\mathrm{CZ}} \rangle$, respectively. First, we observe that the renormalized droplet volume and CZ area are both restricted to the same narrow range 0.5–1.5. Second, despite the statistical noise, a clear correlation between the droplet volume and area of the respective CZ is observed: the larger the CZ area A_{CZ}, the larger the droplet size. A linear relation between $A^{3/2}$ and A_{CZ} [represented by the solid line in Fig. 6(a)] describes well the trend. Similar correlations were found for samples grown at different coverage Θ and T_s.

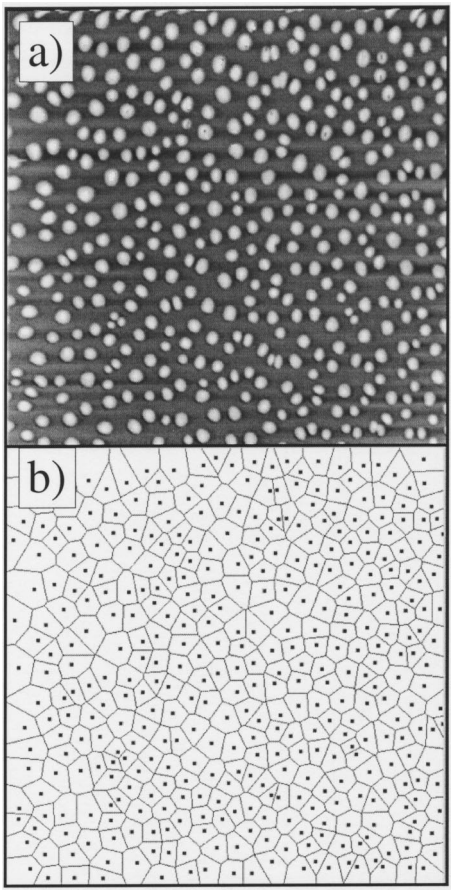

FIG. 5. Voronoi tessellation performed on a 5-nm thin film of Alq_3 grown onto passivated Si(100) at $T_s = 125\,^{\circ}\mathrm{C}$: (a) topography image and (b) computed Voronoi pattern.

The second experimental observation in favor of the CZ growth mechanism is the scaling behavior of the DSD as a function of Θ and T_s.[13] The scaling property of the DSD in the CZ model stems from the invariance of the Voronoi mosaic built on the seed of stable nuclei. In Fig. 6(b), we have depicted the distributions of CZ area obtained from the computed Voronoi pattern and the corresponding distribution of droplet size (volume). As expected for a CZ growth mechanism, both distributions match well. The CZ area distribution obtained from Voronoi tesselation is perfectly fit to a Γ function $G_p(A_{\mathrm{CZ}}/\langle A_{\mathrm{CZ}} \rangle)$ with $p = 10.5$, which compares well with the value obtained from the first and second moments of the distribution of the projected droplet area ($p = 12$).

D. Spatial correlations

1. Emergence of a cutoff distance

The large p value fitting our experimental DSD not only indicates a narrow dispersion of size, but also, in light of the CZ model, points to a spatially correlated Voronoi mosaic. In a true random Voronoi mosaic, built on a Poisson-distributed seed, the analytical form of the DSD is a Γ distribution

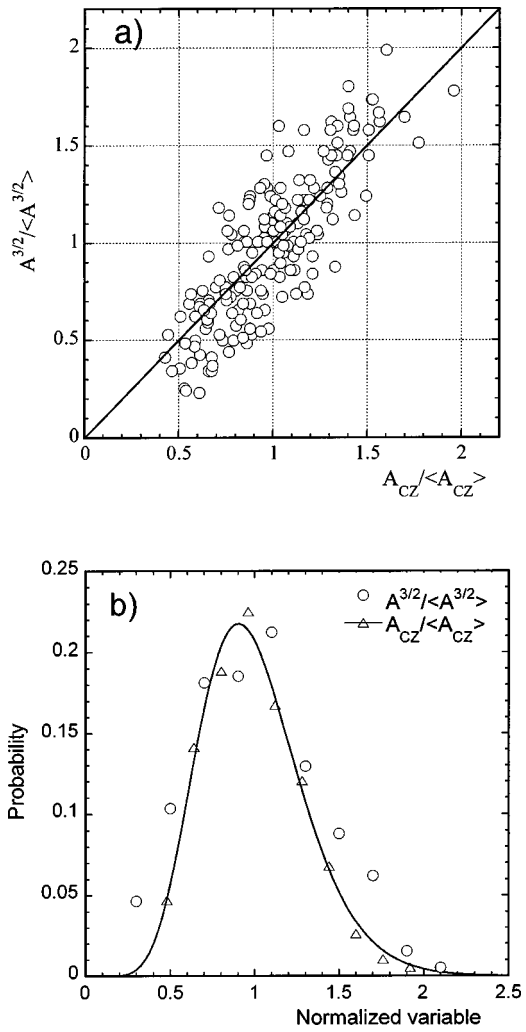

FIG. 6. (a) Correlation between the individual CZ area of droplets and their volume (proportional to $A^{3/2}$ where A is the projected area of the droplet) in the plane of the substrate as obtained from the Voronoi pattern of Fig. 5. Both $A^{3/2}$ and A_{CZ} have been renormalized with respect to their mean values $\langle A^{3/2}\rangle$ and $\langle A_{CZ}\rangle$. (b) Distributions of CZ area and droplet size (volume). The solid line represents the result of a fit of the CZ area distribution using a Γ function $G_p(x)$ with $p=10$.

$G_p(x)$ with $p=3.57$.[32] Deviation from the random mosaic is observed, for instance, when a selection rule of stable nuclei is introduced during the nucleation stage.[21,22]

We have computed various Voronoi mosaics for samples corresponding to different cutoff distances $d_{\min}$ as shown in Fig. 7 and have accordingly calculated the CZ area distributions for various $d_{\min}$ values, shown in Fig. 8. For ease of comparison, we have normalized the cutoff distances $d_{\min}$ relatively to the distance $1/\sqrt{N}$, where N is the density of stable nuclei per unit surface used for the simulation.

We observe that the analytical form of the simulated DSD is perfectly described by a Γ function $G_p(x)$ and preserved for increasing $\mathcal{E}=d_{\min}\sqrt{N}$. Moreover, the DSD is found to narrow significantly with increasing cutoff distance $\mathcal{E}$. The p value characterizing the simulated CZ area distributions with a Γ function is nonlinearly increasing with increasing $\mathcal{E}$. The

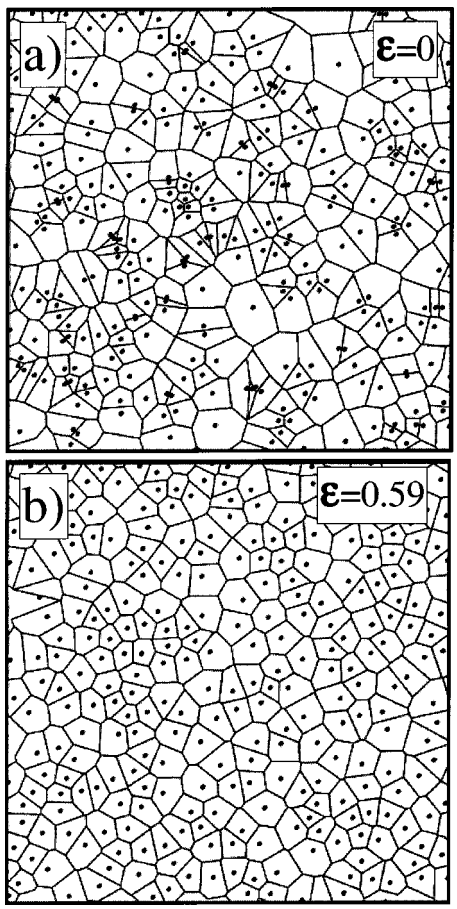

FIG. 7. Simulated Voronoi mosaics for various cutoff distances $\mathcal{E}$. The cutoff distances $d_{\min}$ used for the simulations have been renormalized with respect to $1/\sqrt{N}$ where N is the density of nuclei per unit surface used for the simulation, e.g., $\mathcal{E}=d_{\min}\sqrt{N}$.

asymptotic limit ($\mathcal{E}=2^{1/2}/3^{1/4}\sim 1.07$) for which $p(\mathcal{E})$ diverges corresponds to the hexagonal close packing of a monodispersed system. The experimental value of $p=10\pm 2$ found in our case for the DSD corresponds to a cutoff distance $d_{\min}\sim 0.47/\sqrt{N}\approx 0.1-0.2\ \mu$m, which quantifies the mesoscopic range of spatial correlations.

2. Evolution of spatial correlations with surface coverage

In Ref. 13, we analyzed the spatial correlations of the droplet patterns by using the height-height correlation function obtained from the angularly averaged autocorrelation function of the topography. At constant T_s, the correlation function shows a peak corresponding to the mean nearest-neighbor distance $\langle d_{NN}\rangle$ with damped oscillations related to second next neighbors. The intensity of the main peak was found to increase with increasing coverage, pointing to an enhancement of correlations with increasing coverage Θ. The correlation function at full coverage was found to be typical of systems showing liquidlike order. Here we analyze the spatial correlations by means of the nearest—neighbor distance distribution (NNDD) as a function of coverage.

Figure 9 depicts the evolution of the scaled NNDD, $J(x)=d_{NN}/\langle d_{NN}\rangle)$, as a function of coverage Θ for T_s

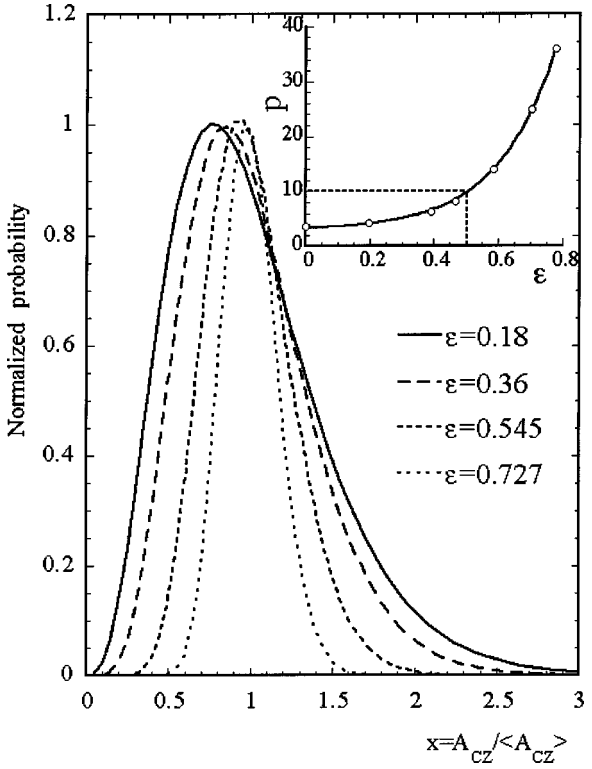

FIG. 8. Calculated CZ area distributions obtained from the Voronoi mosaics simulated for various cutoff distances $\mathcal{E}$. All distributions have been renormalized with respect to their maximum probability. The inset represents the variation of the p factor, obtained from the fitting of the calculated CZ area distributions with a Γ function $G_p(x)$ for a cutoff distance $\mathcal{E}$.

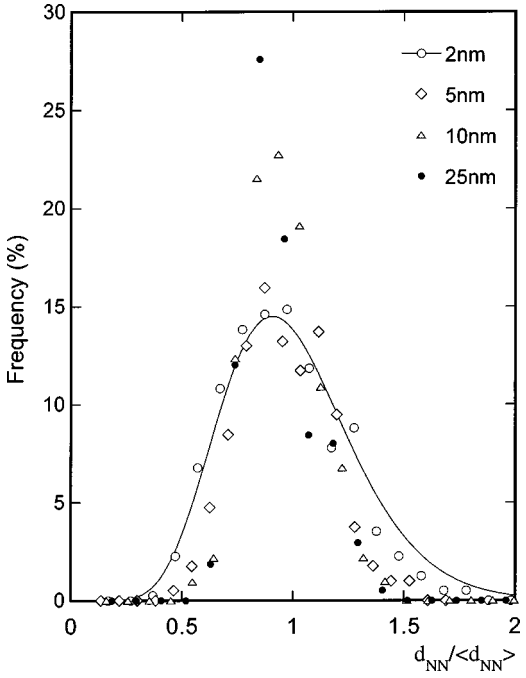

FIG. 9. Evolution of the NNDD $J(x)$ as a function of increasing coverage Θ for thin films grown at $T_s=100\,^{\circ}\mathrm{C}$. The distributions are obtained from the statistical analysis of samples of 400 particles and subsequent binning (20 bins) over the same NN distance interval. x is the rescaled variable, $x=d_{\mathrm{NN}}/\langle d_{\mathrm{NN}}\rangle$. The solid line is the result of a fit using a Γ distribution $G_p(x)$ with variable p for the sample of thickness 2 nm. The values of p obtained by fitting are collected in Table I.

$=100\,^{\circ}\mathrm{C}$. Similarly to the DSD, $J(x)$ is skewed and characterized by a positive third moment. A significant narrowing of the NNDD is observed with increasing Θ, suggesting that spatial correlations appear already at low coverage as the stable nuclei form and increase with coverage. In order to characterize the analytical form of the NNDD, we have estimated the polydispersity ratio $q=\langle d_{\mathrm{NN}}\rangle^2/\sigma^2_{\mathrm{NN}}$ between the mean value $\langle d_{\mathrm{NN}}\rangle$ and the variance σ^2_{NN} of NNDD and compared it with that obtained from a fit of the data with a Γ function. The values obtained for q and the fit are shown in Table I. There is a very good agreement between the values obtained by the two different methods, which indicates that the analytical form of the NNDD is well described by a Γ function. The increase in the q value with increasing Θ (viz, narrowing of the distribution) reflects the existence of an ordering mechanism of the domains in the plane of the substrate, i.e., an increase in spatial correlations between the domains. This result is clear evidence of the peculiar noncoarsening behavior of Alq_3 with respect to systems subjected to significant coarsening, whose NNDD shows an opposite trend.[19,33]

IV. DISCUSSION

A. Nucleation and early stage of growth

In the case of Alq_3 on Si, we can imagine two mechanisms by which a selection of stable nuclei can occur in the early stage of growth ($\Theta<8\%$): (i) the coalescence of close-lying nuclei and (ii) direct ripening.[34] In order to conciliate our observations concerning the kinetics and scale invariance of the DSD, such mechanisms of selection must occur on a short time scale, which means during the very early stage of deposition.

The presence of close-lying nuclei (appearing as very small droplet pairs) is visible for thin films of thickness 2 nm at $T_s=100\,^{\circ}\mathrm{C}$ (see Fig. 1) obtained at $\kappa=1$ nm/min. For samples of thickness 10 nm, such pairs are no longer visible. It is therefore reasonable to consider that initially, i.e., for $\Theta<8\%$, close-lying pairs can merge, introducing in this way a minimum nearest-neighbor distance. Such a mechanism, qualified as direct ripening, can accordingly account for the

TABLE I. Comparison of the value of the ratio $q=\langle d_{\mathrm{NN}}\rangle^2/\sigma^2_{\mathrm{DNN}}$ between the first two moments of the NNDD with the value of q obtained from the fitting of the NNDD with a Γ distribution $G_q(x)=q^{q-1}/\Gamma(q)x^{q-1}\exp(-qx)$ for Alq_3 thin films grown at $T_s=100\,^{\circ}\mathrm{C}$. Here x is the scaled variable $d_{\mathrm{NN}}/\langle d_{\mathrm{NN}}\rangle$.

Film thickness (nm)	Areal coverage (%)	$q=\langle d_{\mathrm{NN}}\rangle^2/\sigma^2_{\mathrm{DNN}}$	q from NNDD fit
2	8	15	14 ± 2
5	19	24	22 ± 2
10	41	37	36 ± 3
25	90	48	38 ± 7

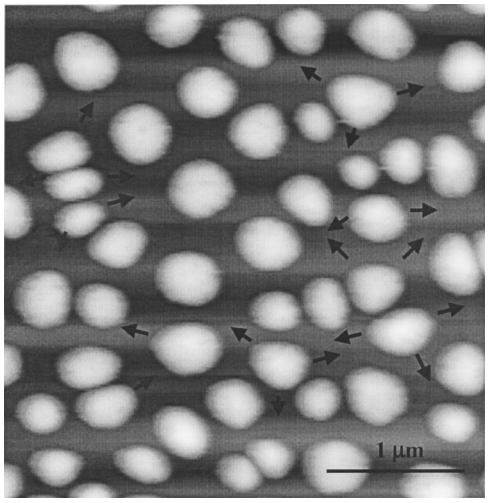

FIG. 10. Topographic image of a 20-nm thin film of Alq_3 deposited onto passivated Si(100) at $T_s = 125\,^{\circ}\mathrm{C}$. The white arrows indicate the directions corresponding to the elongation and deformation of the Alq_3 droplets.

nonrandom distribution of the nearest-neighbor distances.[34] Direct ripening is expected to occur in a short time interval just after nucleation when the diffusion areas around newly formed nuclei overlap. It affects mainly close-lying nuclei and is therefore strongly dependent on the fraction of close-lying droplet pairs. In the present case, it is not possible to discriminate between coalescence of close-lying pairs and direct ripening, which are both expected to lead to a similar cutoff distance between droplets.

B. Evolution of spatial correlations during growth

Various theoretical models have been proposed to explain the occurrence of nonrandom spatial distributions of domains. As from Sec. III D, a nonrandom spatial distribution of domains occurs during the early stage of growth just after nucleation (typically $\Theta < 8\%$ in our case) by the coalescence of close pairs of droplets and/or direct ripening. However, both the evolution of the angularly averaged autocorrelation function[13] and that of the NNDD with increasing Θ clearly show that spatial correlations are further enhanced during growth. The explanation we propose is based on the growth phenomenology described in Ref. 13. As shown in Fig. 10, for films grown at $T_s = 125\,^{\circ}\mathrm{C}$ and a coverage $\approx 30\%$, droplets tend clearly to deform and elongate in the directions corresponding to empty depletion zones. This observation can be simply rationalized in the framework of the CZ model of growth. Figure 11 sketches the mechanism of droplet growth which involves (i) direct incorporation of impinging molecules at the droplet surface (accommodation factor σ_{vl}) and (ii) incorporation of Alq_3 molecules diffusing on the surface of the Si(100) substrate to the periphery of the droplet (accommodation factor σ_{vs}).[13] The arrows of different lengths in Fig. 11(a) represent the total amount of admolecules captured along a given direction in the CZ, which depends on the geometry of CZ cell. Along directions corresponding to large distances to the cell boundaries, more material will be incorporated with respect to the direction of the

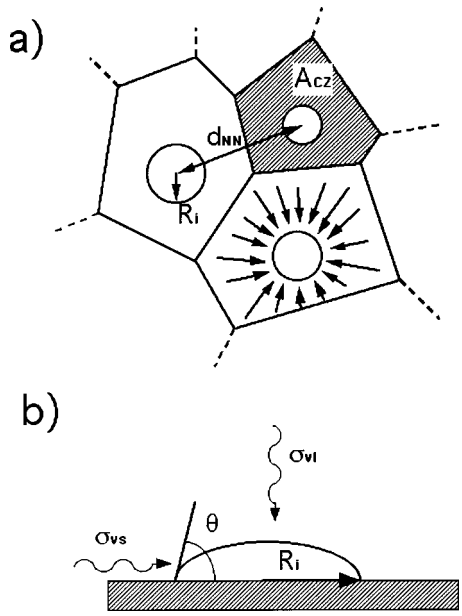

FIG. 11. Scheme of Alq_3 droplet growth on a substrate in a partial wetting regime: (a) Wigner-Seitz cells (area A_{CZ}) are drawn around droplets and correspond to the zero-density flux lines, (b) cross section of droplet of contact angle θ, showing the two competing growth processes: (i) surface diffusion of Alq_3 molecules to the droplet perimeter (accommodation factor σ_{vs}) and (ii) direct incorporation of the incoming flux on the droplet surface (σ_{vl}).

NN, for instance. In the absence of a fast shape relaxation of the droplets, due to the glassy character of Alq_3,[14] a progressive change of the droplet shape will appear, as in Fig. 11. Ultimately, as Θ reaches 100%, the shape of the droplet will approach that of its CZ: i.e., a polygonal shape will be attained as observed, for instance, at $T_s = 150\,^{\circ}\mathrm{C}$ (see Fig. 2 in Ref. 13). Beside the change in shape, the centers of mass of the domains will tend to move in directions corresponding to the empty depleated areas. In this way, a more uniform spatial arrangement develops during the film growth, i.e., a liquidlike ordering of domains can emerge with increasing Θ. This explanation accounts for both the narrowing of the NNDD and the peaking of the height-height correlation function[13] with increasing Θ.

V. CONCLUSIONS

In summary, our results evidence an original growth mechanism whereby an organization of domains is achieved on the mesoscale for a polar molecule sublimed onto an apolar substrate. The peculiarity of the observed growth mode lies mainly in the absence of coarsening phenomena during growth, which leads to spatially correlated droplet patterns with narrow-size distributions and the emergence of a liquidlike order. Homogeneous nucleation occurs in a regime of initially incomplete condensation and is characterized by a critical cluster size $i = 5$. The subsequent growth phenomenology is consistent with the predictions of the CZ model proposed by Mulheran and Blackman.[21,22] Voronoi analysis was used to quantify the degree of order achieved in nonran-

dom droplet patterns. By such analysis, the major assumption of the CZ model—namely, the proportionality between the droplet size and CZ area—has been established. New insight into the early stage of growth has been obtained using numerical simulations of Voronoi mosaics with different cutoff distances. The existence of a minimal cutoff distance between droplets is attributed to the merging of close-lying pairs and/or direct ripening for $\Theta < 8\%$. It results in narrow-size distributions whose analytical form fits with a Γ function $G_p(x)$ with a large p value. Spatial correlations are further enhanced by diffusive interactions between droplets which cause their centers of mass to move towards empty depleated areas. The overall peculiarities of this growth mechanism illustrate how the chemical nature of both the molecule and substrate can be used to achieve an organization of domains at the mesoscale. This work raises more general questions: What is the limit of order achievable in such patterns? Is it possible to obtain spontaneously hexagonal arrays of molecular materials by sublimation using some specific molecule-substrate interactions? Answers to these questions would help to understand, design, and realize ''smart'' molecular systems able to spontaneously organize at multiple length scales, which is one of the most important goals for nanoscience and fabrication.

ACKNOWLEDGMENTS

We acknowledge partial support from EU-TMR programs SELOA FMRX-CT-960083, EUROLED FMRX-CT-970106, LAMINATE HPRN-CT-2000-00135, and CNR-PF-MSTA II ''DEMO.''

*Corresponding author. Email address: F.Biscarini@ism.bo.cnr.it

[1] C. W. Tang and S. A. VanSlyke, Appl. Phys. Lett. **51**, 913 (1987).
[2] Y. Hamada, IEEE Trans. Electron Devices **44**, 1206 (1997).
[3] G. Horowitz and M. E. Hajlaoui, Adv. Mater. **12**, 1046 (2000); F. Biscarini, M. Murgia, M. Cavallini, F. Dinelli, P. Levy, and D. De Leeuw (unpublished).
[4] H. Klapper, M. Kobayashi, T. Kobayashi, and K. Sato, in *Organic Crystals*, edited by H. C. Freyhardt and G. Müller (Springer-Verlag, Berlin, 1991).
[5] S. R. Forrest, Chem. Rev. **97**, 1793 (1997), and references therein.
[6] E. Umbach, K. Glöckler, and M. Sokolowski, Surf. Sci. **404**, 20 (1998).
[7] E. Umbach, W. Gebauer, A. Soukopp, M. Bässler, and M. Sokolowski, J. Lumin. **76**, 641 (1998); M. Buongiorno-Nardelli, D. Cvetko, V. De Renzi, L. Floreano, R. Gotter, A. Morgante, M. Peloi, F. Tommasini, R. Danieli, S. Rossini, C. Taliani, and R. Zamboni, Phys. Rev. B **53**, 1095 (1996); S. Prato, L. Floreano, D. Cvetko, V. DeRenzi, A. Morgante, S. Modesti, F. Biscarini, C. Taliani, and R. Zamboni, J. Phys. Chem. B **37**, 7788 (1999).
[8] J.-C. Wittmann and P. Smith, Nature (London) **353**, 414 (1991).
[9] F. Biscarini, R. Zamboni, P. Samorì, P. Ostoja, and C. Taliani, Phys. Rev. B **52**, 14 868 (1995).
[10] F. Biscarini, P. Samorì, O. Greco, and R. Zamboni, Phys. Rev. Lett. **78**, 2389 (1997).
[11] J. A. Venables, G. D. Spiller, and M. Hanbücken, Rep. Prog. Phys. **47**, 399 (1984).
[12] M. Seul and C. A. Murray, Science **262**, 558 (1993); M. Seul and D. Andelman, *ibid.* **267**, 476 (1995), and references therein.
[13] M. Brinkmann, F. Biscarini, C. Taliani, I. Aiello, and M. Ghedini, Phys. Rev. B **61**, R16 339 (2000).
[14] M. Brinkmann, G. Gadret, M. Muccini, C. Taliani, N. Masciocchi, and A. Sironi, J. Am. Chem. Soc. **122**, 5147 (2000). Alq_3 is a chiral molecule, and the starting material, as well as the thin films, are made of a racemic mixture. All crystal structures resolved exhibit the adjacency of both antiparallel dipoles and D and L enantiomers. The glassy nature of Alq_3 droplets can be understood from the low probability to give rise to crystalline order in nonequilibrium growth conditions.
[15] A. Curioni, M. Boero, and W. Andreoni, Chem. Phys. Lett. **294**, 263 (1998).
[16] D. Beysens and C. M. Knobler, Phys. Rev. Lett. **57**, 1433 (1986).
[17] D. Fritter, C. M. Knobler, D. Roux, and D. Beysens, Phys. Rev. A **43**, 2858 (1991).
[18] J. L. Viovy, D. Beysens, and C. M. Knobler, Phys. Rev. A **37**, 4965 (1988).
[19] D. Fritter, C. M. Knobler, D. Roux, and D. Beysens, J. Stat. Phys. **52**, 1447 (1988).
[20] M. Zinke-Allmang, L. C. Feldman, and M. H. Grabow, Surf. Sci. Rep. **16**, 377 (1992).
[21] P. A. Mulheran and J. A. Blackman, Philos. Mag. Lett. **72**, 55 (1995).
[22] P. A. Mulheran and J. A. Blackman, Phys. Rev. B **54**, 11 681 (1996).
[23] J. A. Venables and D. J. Ball, Proc. R. Soc. London, Ser. A **332**, 331 (1971).
[24] J. A. Stroscio and D. T. Pierce, Phys. Rev. B **49**, 8522 (1994).
[25] N. Hirashita, M. Kinoshita, I. Aikawa, and T. Ajioka, Appl. Phys. Lett. **56**, 451 (1990).
[26] J.-F. Moulin, M. Brinkmann, A. Thierry, and J.-C. Wittmann, Adv. Mater. **14**, 436 (2002).
[27] C. Icking, R. Klein, P. Köllner, and L. Ma, Computer code VOROGLIDE, Fern Universität Hagen, 1996–1997.
[28] J. A. Buyers, J. Anim. Ecol. **61**, 759 (1992).
[29] M. C. Bartelt and J. W. Evans, Phys. Rev. B **46**, 12 675 (1992); M. C. Bartelt, M. C. Tringides, and J. W. Evans, *ibid.* **47**, 13 891 (1993).
[30] J. A. Venables, Philos. Mag. **27**, 697 (1973).
[31] K. Hartig, A. P. Janssen, and J. A. Venables, Surf. Sci. **74**, 69 (1978).
[32] D. Weaire and N. Rivier, Contemp. Phys. **25**, 59 (1984); D. Weaire, J. P. Kermode, and J. Wejchert, Philos. Mag. B **53**, L101 (1986).
[33] G. R. Carlow and M. Zinke-Allmang, Phys. Rev. Lett. **78**, 4601 (1997); G. R. Carlow, R. J. Barel, and M. Zinke-Allmang, Phys. Rev. B **56**, 12 519 (1997).
[34] E. Ruckenstein and D. B. Dadyburjor, Thin Solid Films **55**, 89 (1978).